Materials Today • Volume xxx, Number xx • xxxx 2020 RESEARCH

ELSEVIER

RESEARCH: Original Research

Reliable mechatronic indicator for self-powered liquid sensing toward smart manufacture and safe transportation

Jie An [1,2,†], Ziming Wang [1,2,†], Tao Jiang [1,2,†], Pengfei Chen [1,2], Xi Liang [1,2], Jiajia Shao [1,2], Jinhui Nie [1,2], Minyi Xu [3,*], Zhong Lin Wang [1,2,4,*]

[1] CAS Center for Excellence in Nanoscience, Beijing Key Laboratory of Micro-nano Energy and Sensor, Beijing Institute of Nanoenergy and Nanosystems, Chinese Academy of Sciences, Beijing 100083, China
[2] School of Nanoscience and Technology, University of Chinese Academy of Sciences, Beijing 100049, China
[3] School of Maritime Engineering, Dalian Maritime University, Dalian 116026, China
[4] School of Materials Science and Engineering, Georgia Institute of Technology, Atlanta, GA 30332-0245, USA

In the era of industry 4.0, mechanical indicators are in great demand for providing reliable information in a harsh environment with a self-powered signal transmission ability for connecting into a centralized automatic control network of ships, trucks, and factories. In this work, based on the principle of nanogenerator, we report a block-inserting mechatronic (BIM) panel employed as not only a mechanical indicator with long operation lifetime, versatile adaptability, and improved reliability under harsh working conditions, but also an active electronic sensor for self-powered liquid information indicating and sensing. The methodology of block-inserting assembly significantly simplifies the processing costs and difficulties, which facilitates length-customization of the whole device. When equipped with the BIM panel, computer control and monitoring systems realize wireless control and real-time monitoring of liquids in miscellaneous industrial applications. This work lays the foundation of nanogenerator-based sensors applied in industrial systems, which will strongly promote the progress of industry 4.0, smart cities, and transportation.

Introduction

With the rapid development of technologies for internet of things (IoTs), big data, and artificial intelligence (AI), the lifestyle of humans has been fundamentally reshaped due to the booming fields of personalized healthcare [1,2], smart home, and automatic driving. Modern industry will gradually enter the era of intelligent manufacturing, in which equipment operates automatically and continuously under the regulation of a central artificial intelligent controller without human supervision, rescuing staffs from harsh and hazardous working environments. However, the combination with big data and AI technologies would be very difficult without the assistance of numerous distributed electronic sensors. These sensor networks relying on electricity not only cause energy consumption but also complicate the device structure and endanger the system stability and maintainability. Therefore, there is an urgent need to develop an active sensing strategy that could directly generate sensing signals under external mechanical agitations.

Petroleum, water, chemical solutions, and other liquid raw materials are often regarded as the blood of modern industry, which have been widely exploited in fields of petroleum exploitation, chemical engineering, and sewage purification [3]. However, in practical industrial applications, liquid sensors need to be reliable and adaptable to high temperature, high pressure, corrosion, and other harsh working conditions with features of adequately long service lifetime and easy troubleshooting, which severely limits the applications of electronic liquid sensors in

* Corresponding authors.
E-mail addresses: Xu, M. (xuminyi@dlmu.edu.cn), Wang, Z.L. (zlwang@gatech.edu).
† These authors contributed equally to this work.

 https://doi.org/10.1016/j.mattod.2020.06.003

Please cite this article in press as: J. An et al., Materials Today (2020), https://doi.org/10.1016/j.mattod.2020.06.003

industrial environment [4,5]. The automation in intelligent manufacturing strongly relies on electronic sensors, and mechanical indicators are also introduced into most industrial devices with electronic sensors to achieve intelligent automation and improved reliability [6]. Nevertheless, in these devices, mechanical and electronic sensors are independent of each other, which not only complicates the maintenance process but also greatly increases the fabrication cost. Therefore, there is still a need for an electromechanical integrated liquid sensor with a wide adaptation spectrum, high reliability, and long service life.

Recently, triboelectric nanogenerators (TENGs) have been developed as a promising technology for converting mechanical motions into electrical signals with high sensitivity, quick respondence, and accordance with mechanical motions [7,8]. Hence, they have been utilized as active sensors for tactile sensing, motion monitoring in robotics, and IoT applications without electric energy supply [9–15]. Owing to the merits of active sensors, processors could be activated merely by motion-induced sensing signals and fall into sleep state when no signal is detected [16]. This feature is beneficial to further lower the entire power consumption of the device, and possibly to realize a self-powered system through scavenging ambient distributed mechanical energy [17–23].

Herein, combining the advantages of TENG-based sensors and block inserting assembly, a self-powered block-inserting mechatronic (BIM) panel is constructed. Assisted by a magnetic floater, the BIM panel can act as a reliable mechanical indicator to directly reflect the sensed level and flow characteristics by the visible color variance of flaps, and also as an electronic sensor for automatic control and remote wireless monitoring. Its working principle is revealed by solving Wang's theoretical equations of TENG in a polar coordinate system. The panel is isolated from liquids by magnetic coupling transmission, which is beneficial for liquid monitoring with long operation life and adaptability to harsh working conditions. The block-inserting assembly method could reduce the fabrication cost and simplify the length-customization procedure. The TENG, which ensures exact correspondence between the flap movement and generated electric signals, can produce stable voltage signals even with slight changes of liquid level and flow rate. The voltage step signal will not be influenced by the fluctuation of voltage amplitude, which ensures the measurement accuracy and reliability of BIM panel. Integrated with the BIM panel, a liquid level two-position control system and a flow rate wireless monitoring system are established to realize the precise real-time acquisition and automatic control of the liquid level and flow rate. Finally, a practical boiler feed tank level monitor system on marine equipment is constructed for water level monitoring of marine systems anytime and anywhere through the developed mobile applications. This work provides a new strategy for the TENG-based active sensors applied in liquid-related monitoring and control. Based on the method of this study, various block-inserting mechatronic sensors in a wide range of application fields can be invented, which will promote the development of big data and IoTs for application in smart industries, cities, and transportation.

Material and methods

The BIM panel was assembled from three kinds of building blocks by block-inserting assembly method, including electrode building blocks, flap blocks, and supporting blocks. The flap block was composed of a 3D-printed body, a porous FEP film, and a cylindrical magnet inserted vertically. The porous FEP films were prepared by inductively coupled plasma (ICP) etching process. The etching gas was a mixture of O_2 and Ar gases with a ratio of 95:5. A 400 W power source for generating plasma and a 100 W power for accelerating the plasma ions were used. The etching time was 60 s followed by dipping it into PTFE aqueous emulsion to embed the nanoparticles in the cavity. The electrode blocks on both sides of the flap blocks were processed using printed circuit board (PCB) technology and were designed into the desired shape. Twelve electrode blocks and two supporting blocks were pieced into the device skeleton. Six flap blocks were installed into the device skeleton and made up the entire device with six flap units, each of which could rotate around its axis. The FEP film and two copper electrodes on the PCB blocks formed a free-standing TENG, and six TENG units were connected in parallel by Cu wires for signal transmission. The BIM panel, data acquisition (DAQ) board, computer program (constructed based on LabVIEW), and mobile application (designed by E4A) make up the remote monitoring and control system. Owing to the limited charges of TENG, a voltage integrating circuit is equipped on the DAQ board to prevent charges loss. Microcomputer (STM32F407ZGT6) and WIFI module (esp8266) are equipped to obtain the floater's location through internal program analysis and communicate with terminal equipment to realize remote monitoring and control.

Result and discussion

Structure and fabrication process of BIM panel

The constructed BIM panel is based on the TENG technology and magnetic coupling principle. By coupling their advantages, the panel could not only mechanically indicate liquid position without direct contact with liquids, but also generate corresponding voltage signals for remote transmission, which can find extensive applications in transportation, petrochemical industry, and sewage purification. Fig. 1a depicts prospective applications of the BIM panel in vessels for liquid level and flow rate monitoring. The introduction of the panel could not only enable crews to inspect and regulate the liquid level and flow rate directly according to the indication of color variance of flaps on the panel (Fig. 1c), but also convert buoyance-induced mechanical movements into electrical signals through the TENG technology, facilitating remote monitoring and electric control of equipment (Fig. 1b). The detailed structure of liquid-level meter equipped with BIM panel is visualized in Fig. 1e. In this illustration, the entire device can be mainly divided into two parts: a magnetic floater and an indicator panel consisting of several magnetic flap units. Each unit is composed of a magnetic flap with a cantilever slab (made up of 0.2 mm-thick FEP film as electrification layer) embedded in it (Fig. S1a–c), and a pair of copper electrodes (thickness of 50 μm) distributed on both sides (detailed fabrica-

Please cite this article in press as: J. An et al., Materials Today (2020), https://doi.org/10.1016/j.mattod.2020.06.003

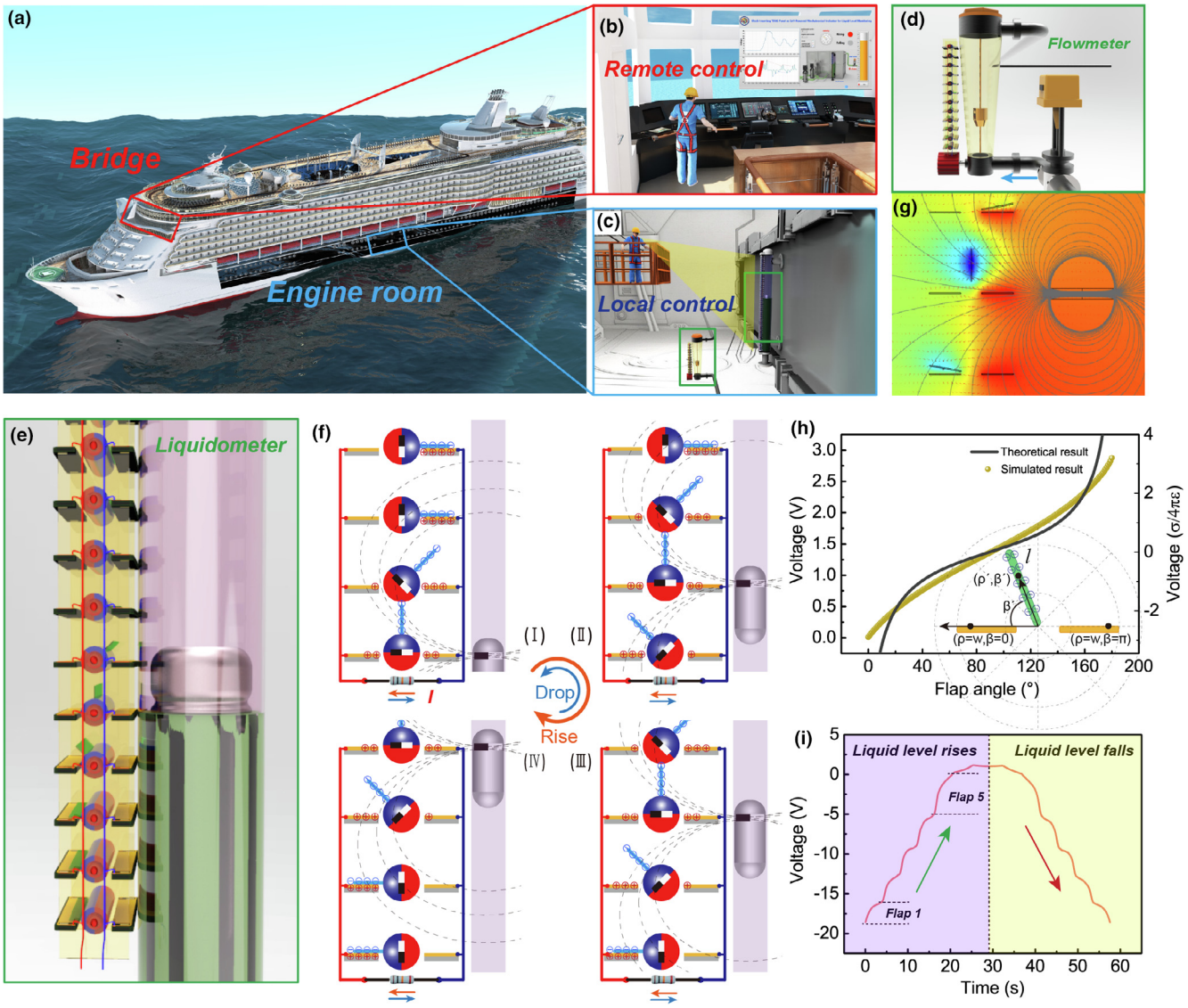

FIGURE 1

Schematic application and structure for the BIM panel. (a) A proposed conceptual application of liquidometer in maritime engineering. (b and c) Enlarged views of (b) bridge room and (c) engine room where crews could monitor the liquid level of oil tank remotely and locally. (d and e) Enlarged structures of (d) BIM flowmeter and (e) liquidometer in engine room. (f) Schematic diagram of the TENG under short-circuit condition when the liquid level rises or drops, where the red and blue arrows respectively indicate the rising and falling processes of liquid level as well as the current flow directions. (g) Simulated electric field and magnetic field distributions at a certain moment through the COMSOL software. The red arrows and rainbow chart depict the electric field direction and electric potential values, respectively, while the gray lines denote the magnetic field lines of the floater. (h) Simulated and theoretical voltage of one TENG when the flap plate flips from left to right. Inset is its schematic diagram of theoretical analysis in polar coordinate system. (i) Voltage signal generated by the liquidometer when the floater first rises and then drops.

tion process is available in Materials and Methods section and Fig. S1d). All the electrodes on the same side of flaps are connected in series and finally form a pair of signal lines for actively transmitting liquid level signals to remote controllers. Besides the liquid level, flow rate is another important fluid parameter that needs to be monitored. Because the positions of the internal floaters can directly reflect the flow rate of the incoming fluid through the cone chamber, the BIM panel can also indicate the flow rate both mechanically and electronically as the BIM liquidometer does (Fig. 1d), exhibiting the wide application spectrum for the BIM panel.

Working condition and operation principle of BIM panel

The magnetic operation principle of the panel is illustrated in Fig. 1f. As the liquid level rises, indicated by the red arrow, the magnetic floater is driven to rise by the buoyancy, inducing the flaps to flip from right to left gradually under the combined actions of magnetic force and gravity. Owing to the larger magnetic force relative to the gravity, the flaps near the magnetic floater will flip for a certain angle, while the flaps far away from the floater will fall on the electrodes under gravity. The flap is painted with red and blue colors on its two sides, respectively, and thus the flaps above the floater remain in red, while those

Please cite this article in press as: J. An et al., Materials Today (2020), https://doi.org/10.1016/j.mattod.2020.06.003

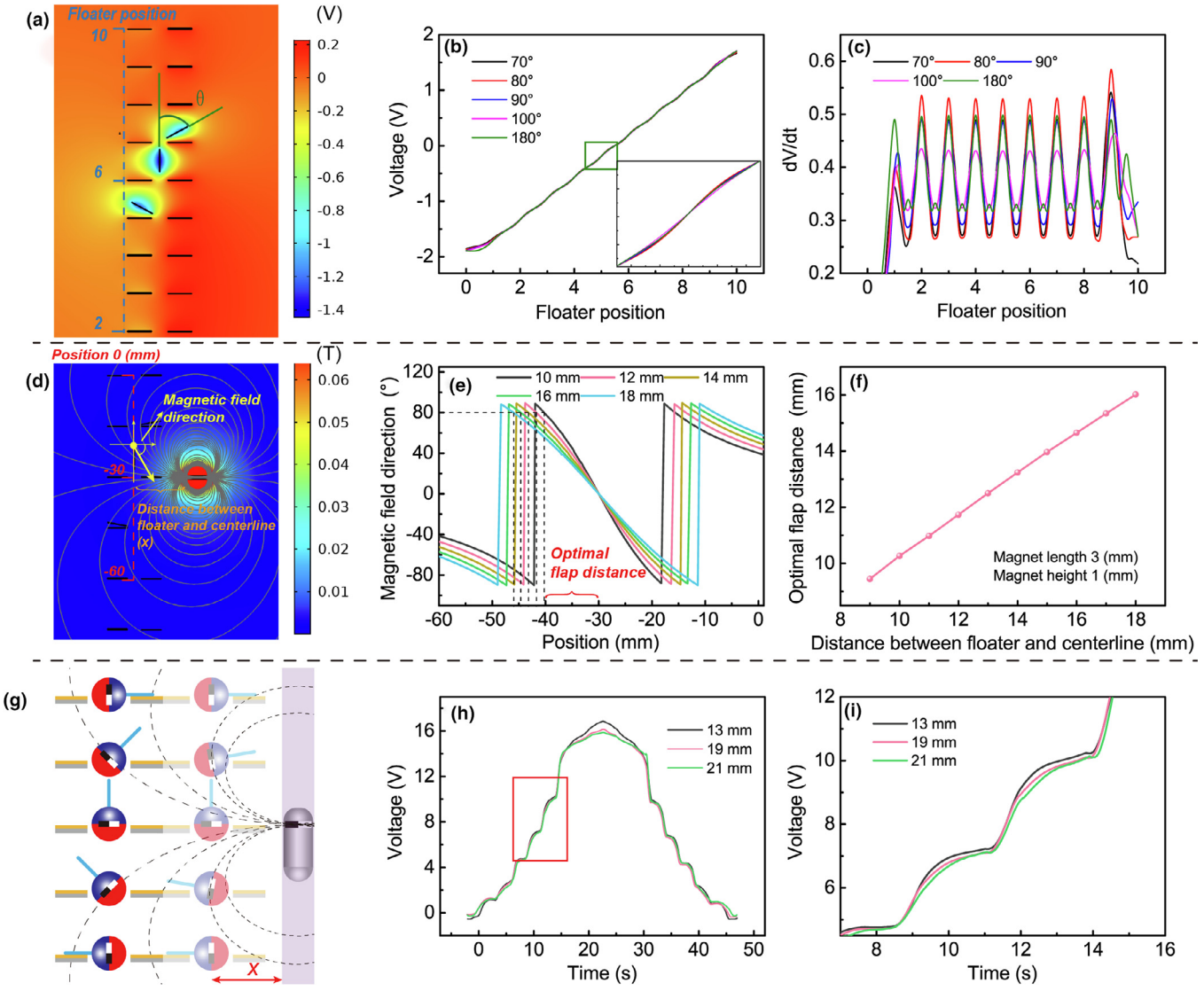

FIGURE 2

Simulation analysis and experimental verification of important factors affecting the sensor's remote transmitted signal. (a) Simulated electric potential distribution at the moment when the floater arrives at position 6. The angle θ is defined as the flipping angle between two adjacent flaps. (b) Calculated open-circuit voltage and (c) differential of the voltage with respect to the time (d*V*/d*t*) at different θ values during the rising process of the floater. (d) Simulated magnet field distribution of the magnet in the floater at a certain moment. The color and line represent the strength and direction of the magnetic field, respectively. (e) Magnetic field direction on flap centerline as a function of the position for different distances *x* between the floater and centerline. (f) Summarized relationship between the optimal flap distance and *x*. (g) Schematic illustration of the flap state at two different positions away from the floater. (h) Experimental voltage signals measured for different distances *x*, and (i) local enlarged view for the voltage profiles during a rising-falling cycle.

below the floater rotate to exhibit blue. Consequently, the floater position can be intuitively visualized by the color difference between flaps. Note that the pipe with the floater inside is made of high-strength metal in practical situations, and the transparent pipe in Fig. 1e is merely utilized to clearly illustrate the correspondence between magnetic flaps and floater. Subsequently, the flipping motion will be transformed into electrical signals using TENG technology. In this process, the FEP cantilever slabs tend to gain electrons from copper during contacts, according to the triboelectrification series [24]. When the flaps flip from the right to the left, positive charges will transfer from the right electrodes to the left ones driven by the potential difference between two electrodes [7,25–28]. The electric potential distribution between two electrodes and magnetic induction lines generated by the magnetic floater were revealed via COMSOL Multiphysics simulations (Fig. 1g).

Theoretical analysis of stepped voltage signal generation

The potential distribution in space can be theoretically derived from expanded Maxwell's equations [8]:

$$\psi(\vec{r},t)=\frac{1}{4\pi\varepsilon}\int\frac{\sigma\left(\vec{r'},t\right)+\sigma_T\left(\vec{r'},t'\right)}{\left|\vec{r}-\vec{r'}\right|}d\vec{s'} \quad (1)$$

For a flap plate with length l and charge density σ, we can easily write down the charge density in polar coordinate system (inset of Fig. 1h):

$$\sigma(\vec{r},t)=\sigma\delta(\beta-\beta') \quad 0\leqslant\gamma\leqslant l \quad (2)$$

Please cite this article in press as: J. An et al., Materials Today (2020), https://doi.org/10.1016/j.mattod.2020.06.003

where (γ, β) is any point in space, (γ', β') is the point on the flap plate, and $\delta(\beta - \beta')$ is a delta function that is introduced to confine the charges on the flap plate.

The potential difference between two opposite points on electrodes is:

$$\psi_2 = \psi_1 = \frac{-\sigma}{4\pi\varepsilon}\int_0^l d\gamma' \left\{ \frac{1}{\sqrt{\left(w-\gamma'\cos\beta'\right)^2+\left(\gamma'\sin\beta'\right)^2}} - \frac{1}{\sqrt{\left(-w-\gamma'\cos\beta'\right)^2+\left(\gamma'\sin\beta'\right)^2}} \right\} = \frac{-\sigma}{4\pi\varepsilon}\ln\frac{\left(l-w\cos\beta'+\sqrt{l^2+w^2-2lw\cos\beta'}\right)\left(\cos\beta'+1\right)}{\left(l+w\cos\beta'+\sqrt{l^2+w^2+2lw\cos\beta'}\right)\left(1-\cos\beta'\right)} \tag{3}$$

The detailed derivation process can be found in Note S1. In Eq. (3), ψ_1, ψ_2 are the electric potentials for the two points of (w, 0) and (w, π) on electrodes, and (γ', β') is the coordinate of points on the flap plate. From this equation we can find that larger charge density σ will generate higher a potential difference, and the calculated voltage is roughly consistent with the simulated result at the flipping process for a flap unit (Fig. 1h), which proves the validity of our theory. The subtle difference between two results derives from the exclusion of charges in electrodes in analytic calculation, due to which these charges can redistribute in electrodes and flatten the theoretical result of voltage.

Because all flap units are connected into a line, a phase difference ϕ exists between the voltage signals from two adjacent flaps when the floater passes through each flap unit in turn. The open-circuit voltage of the BIM panel with N flap units follows the equation

$$V_{OC} = \frac{\sum_{n=1}^{N} Q_{SC,n}}{NC} = \frac{1}{N}\sum_{n} V_{OC,n} \tag{4}$$

where C is the capacitance of each flap unit and $Q_{SC,n}$ denotes the short-circuit transferred charge for the n-th flap unit. According to Eq. (4), the output voltage signal exhibits a stepwise change as shown by the experimental result in Fig. 1i, where the voltage rises and falls synchronously with the liquid level, having the same step number as the flipped flap number.

Based on the above-mentioned analysis of operation principle of the BIM panel, the position signal of magnetic floater could be visually recognized and remotely transferred. Without contact with BIM panel and liquids, the BIM liquidometer and flowmeter can indicate the liquid level and flow rate information according to the floater position. Besides, the applications of BIM panel can be extended to other scenarios as displacement-indicator through reasonable structural designs.

The parameter determines the apparency of voltage steps

As the signal transmission of the BIM panel is based on the transformation of magnetic floater position into stepwise voltage signal, the more evident the step of voltage signal is, the more convenient it is for the processor to analyze the floater position. The waveform of output voltage is the superposition of multiple identical waveforms with a phase difference, which greatly influences the voltage waveforms (the calculation process of superposition can be found from Fig. S2 and Note S2). When defining the angle between the central flap and adjacent flap as θ, as shown in Fig. 2a, the step shape of output signal mainly depends on the θ value, which is associated with the distance between adjacent flap units as well as the magnetic field shape of floater. The electric potential distributions for different θ angles were simulated by COMSOL when the magnetic floater rises as depicted in Fig. 2a and Movie S1 (Fig. 2a shows the case when the floater arrives at position 6). The open-circuit voltage profiles for various θ ranging from 70° to 180° at the rising and falling process of the floater are shown in Fig. 2b and Fig. S3, indicating that the step is more evident at $\theta = 80°$, although there is only a slight difference for different θ (inset of Fig. 2b). That is further verified by the derivation dV/dt of voltage signal (Fig. 2c), which also reaches its maximum value at $\theta = 80°$. Therefore, $\theta = 80°$ is defined as the optimal angle. Moreover, the step positions of voltage signal can be precisely identified from the crests of dV/dt profile. The abnormal crests at both ends of dV/dt are ascribed to the difference in moving flap numbers at the beginning and end points from that at the middle position, which can be addressed in practice by choosing longer panels than the floater movement distance.

Structural optimization of BIM panel

The optimal angle θ is determined by the magnetic field distribution generated by the floater, as the magnet in each flap tends to be arranged along the magnetic field direction at its location. The magnetic field distribution at the moment that the floater arrives at the −30 mm position is shown in Fig. 2d. The optimal flap distance is the distance between the flap at −30 position and the adjacent flap where the magnetic field direction is 80° relative to the horizontal direction, which is determined by the distance x between floater and centerline as well as the magnetic field shape of floater. Fig. 2e shows the magnetic field direction on centerline at various x values, and the optimal flap distances for different x values are extracted and plotted in Fig. 2f. As can be seen, the increase in distance between the floater and centerline results in the divergence of the magnetic field on the centerline followed by a linear increase of the optimal flap distance. The magnetic field shape of the floater is another dominating parameter influencing the optimal flap distance, and thus the size and magnetic flux of the magnet in the floater are studied as shown in Fig. S4a and b. In order to verify these simulation results, a corresponding experiment has been carried out. Through the method of iron power tracing (Fig. S4c), the optimal angle $\theta = 80°$ is roughly measured when the vertical flap distance is 16 mm and the magnetic floater is 13 mm away from the panel centerline. Therefore, if the flap panel is taken away from the magnetic floater, the θ will decrease and deviate from the optimal value of 80° (Fig. 2g), and the step of voltage signal will gradually become flattened (Fig. 2h and i), which is consistent with the simulation result.

Characterizations of BIM panel

A linear motor was functioned as the floater driver to simulate the liquid buoyancy in the sensor characterizations due to its convenience and accuracy of speed control (Fig. 3a). It is of great significance to establish a reliable and facile strategy to process the signals generated by our sensor to acquire the position of the floater. The number of steps and the variance trend of the voltage are two essential parameters determining the floater position. Through the differentiation of the voltage signal, step posi-

Please cite this article in press as: J. An et al., Materials Today (2020), https://doi.org/10.1016/j.mattod.2020.06.003

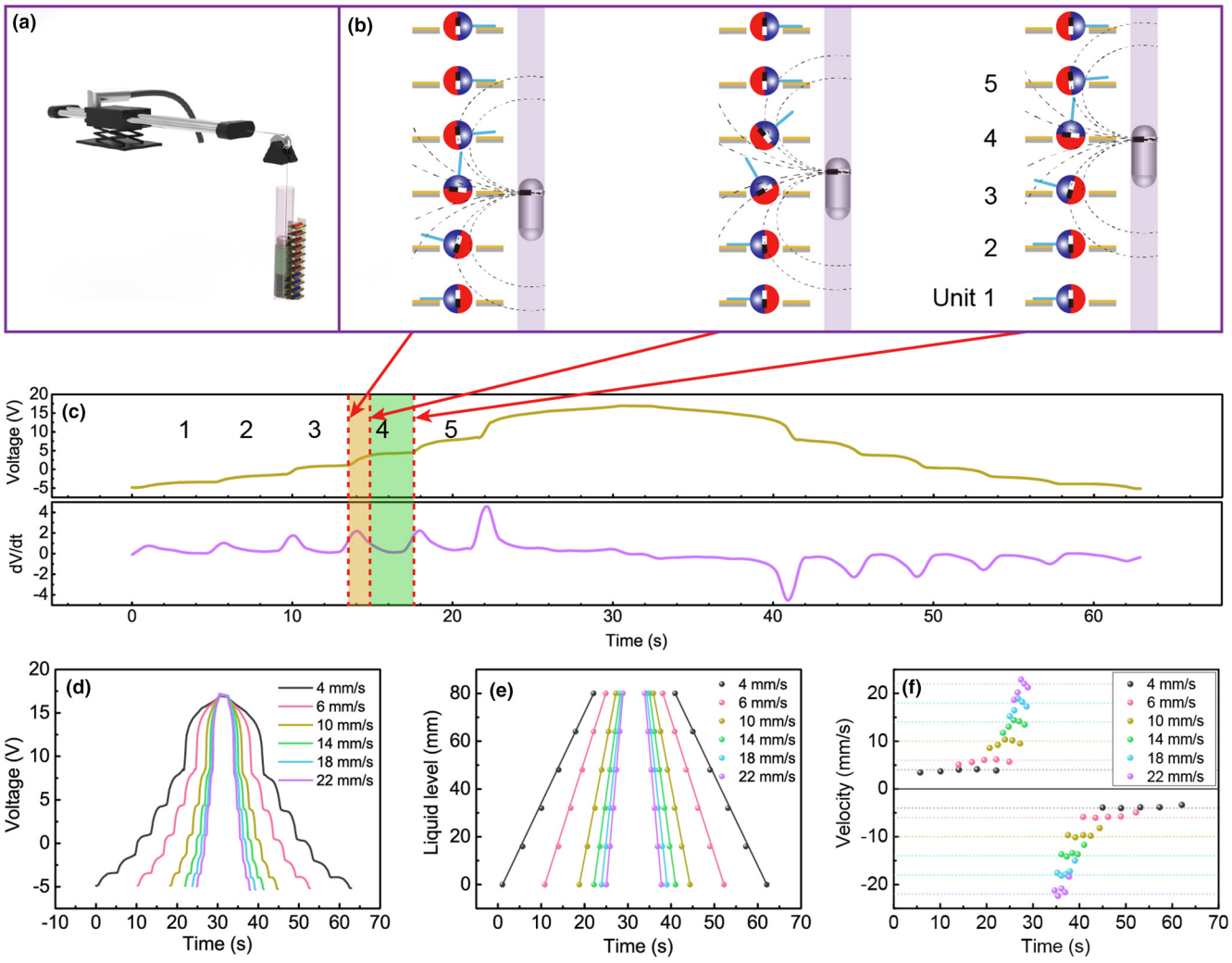

FIGURE 3

Characterization of remote transmitted signal. (a) Schematic diagram of the experimental equipment. (b) Sketch of three typical flap states for the liquidometer. (c) Generated voltage signal and d*V*/d*t* curve in a rising-falling cycle of the floater, where the three typical states are marked. (d) Experimental voltage signals, (e) measured liquid levels compared with the actual levels, and (f) measured rising/falling velocities of the liquid level compared with the actual velocities at different experimental velocities. The colored points represent the measured level and velocity according to the voltage signals of liquidometer, while the solid lines and dot lines represent the actual level and velocity, respectively.

tion and variance trend of voltage signal can be clearly deduced from the crests of d*V*/d*t* and its sign (positive or negative) (Fig. 3c). Subsequently, comprehensive experiments of voltage signal acquisition and analysis at different rising and falling speeds of the magnetic floater were carried out. The device was equipped with 6 magnetic flaps and the flap distance is an optimal 16 mm. As presented in Fig. 3d and Fig. S5, an identical number of voltage steps are obtained when the magnetic floater moves for the same distance at different speeds. Each voltage step represents a floater movement of 16 mm that corresponds to the distance between two flaps. By counting the number of d*V*/d*t* peaks (Fig. S6a), the liquid level value at each moment can be calculated (Fig. 3e). The liquid level measured by the BIM panel is almost linear with time with the maximum error of only 0.125% (Fig. S6b) when the floater moves at a constant speed (the points are the measured floater level and the solid line is the actual value). Further, its moving velocity can also be calculated by dividing the displacement by the spent time. Fig. 3f shows the relationship between measured velocity (colored points) and the actual preset one (dot lines) at different moving speeds of the floater. It can be found that the measured value is in good agreement with the real value when the floater speed is lower than 6 mm/s. Even if the speed exceeds this value, the measuring error will only increase slightly (Fig. S7 and Note S4). It is worth emphasizing that a higher measuring accuracy of liquid level and velocity can be obtained by reducing the flap distance. However, for practical applications, the height of measured tank (H) is more than 2 m, which is much longer than the distance between flaps. In this case, the maximum measurement error (err_{max}) is only 0.8% for the devices with the flap distance (Δd) of 16 mm via the following expression:

$$err_{max} = \frac{\Delta d}{H} \tag{5}$$

which is far beyond the practical measurement accuracy required. In addition, owing to the large bottom surface of the water tank,

Please cite this article in press as: J. An et al., Materials Today (2020), https://doi.org/10.1016/j.mattod.2020.06.003

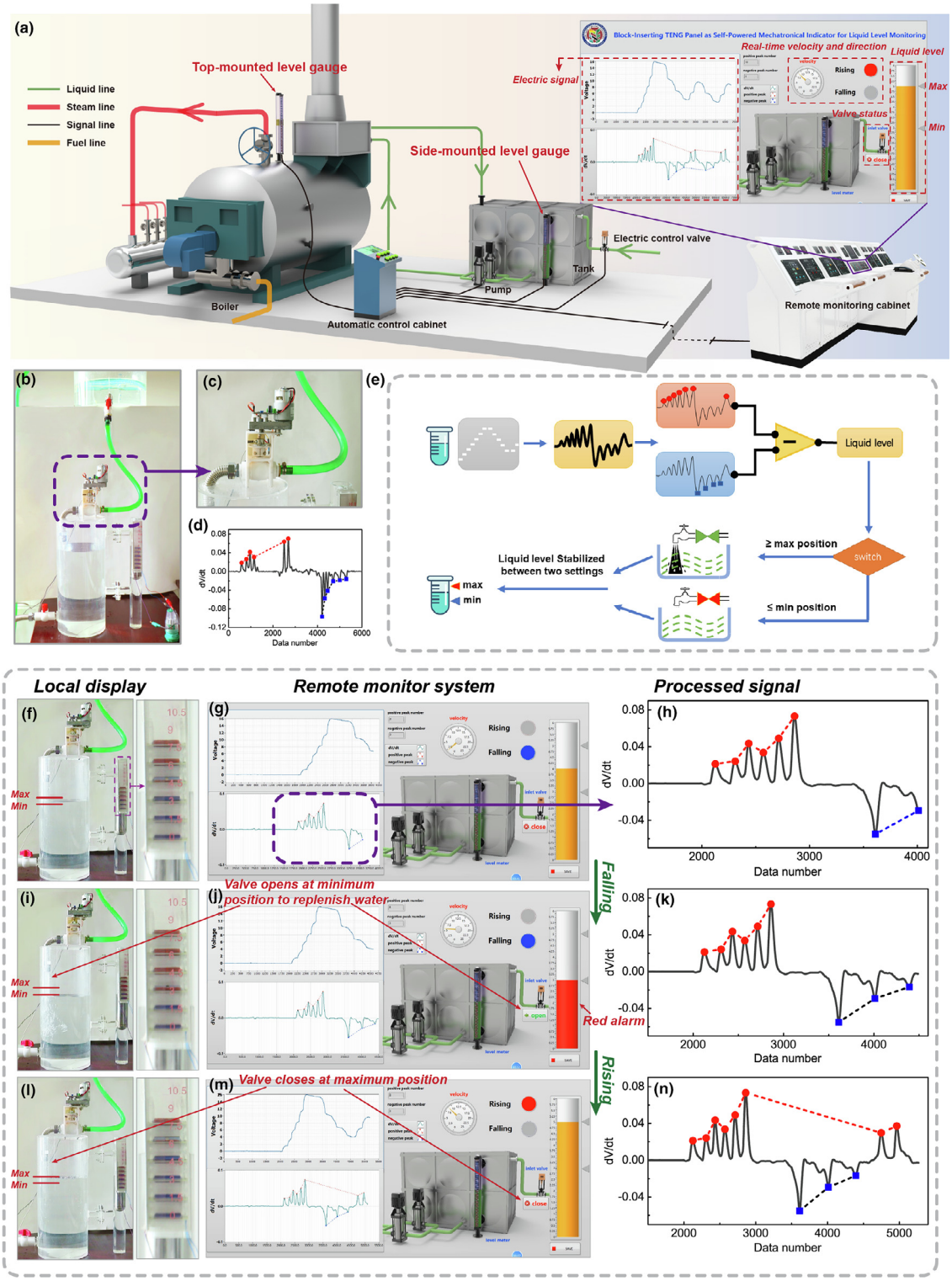

FIGURE 4

Application of BIM indicator panel in liquid level monitoring. (a) Schematic diagram of a conceptual boiler feed water system equipped with two kinds of BIM liquidometers (top-mounted type and side-mounted type). (b) Photograph of a simulated tank feed system. (c) Enlarged view of the electrical control water valve. (d) d*V*/d*t* signal of the liquidometer acquired by the computer-side monitoring program. (e) Schematic illustration of the obtaining of real-time liquid level information by analyzing positive and negative peaks of processed d*V*/d*t* signal, followed by the stabilization of the liquid level between two settings through the automatic opening of the inlet valve to replenish water. (f) Photograph of the liquidometer equipped on the water tank. (g) Program interface of the remote liquid level monitoring and control system, and (h) diagram of processed real-time d*V*/d*t* signal when the water level descends to a certain position. (i–k) Status of machine side and remote-control side as well as diagram of processed d*V*/d*t* signal when the water level falls to the low setting level. At that moment, the remote control system sends a red alarm signal and opens the inlet valve to replenish water. (l–n) Status of machine side and remote-control side, and processed d*V*/d*t* signal when the water level rises to the maximum position. The remote control system sends commands to close the inlet valve to finish replenishment.

Please cite this article in press as: J. An et al., Materials Today (2020), https://doi.org/10.1016/j.mattod.2020.06.003

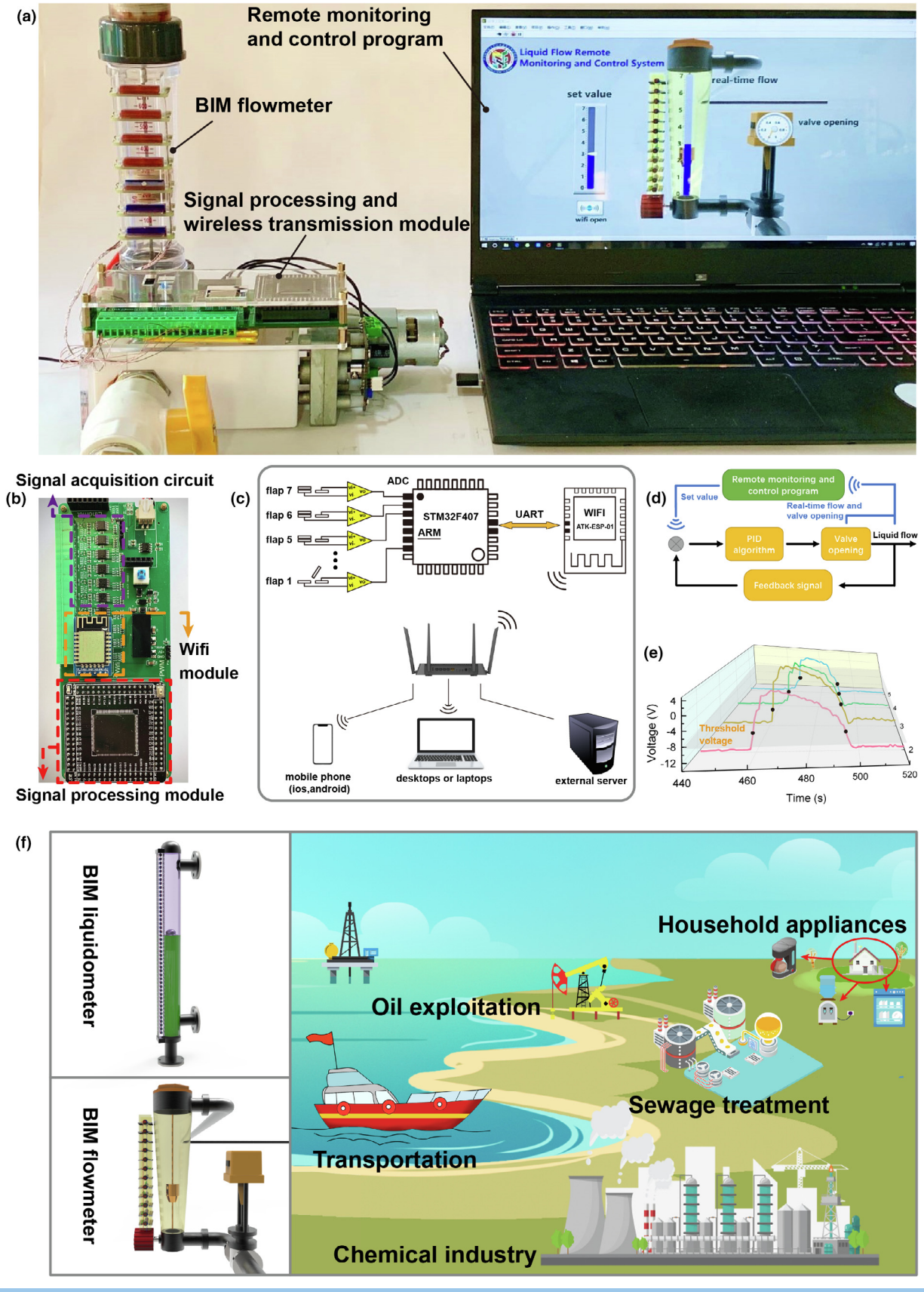

FIGURE 5

Wireless liquid flow monitoring and control system supporting the expansion of IoTs in industrial fields. (a) Panorama of the wireless flow rate control system including the BIM flowmeter, integrated signal processing, and wireless transmission circuit board, electric control valve as well as remote monitoring and control program. (b) Enlarged photograph of the integrated signal processing and wireless transmission circuit board. (c) Schematic circuit diagram and (d) wireless control and monitoring flow chart of liquid flow rate in this system. (e) Voltage signals of four channels acquired by the integrated signal processing and wireless transmission circuit board. (f) Application prospects of the BIM liquidometer and flowmeter in different scenarios.

Please cite this article in press as: J. An et al., Materials Today (2020), https://doi.org/10.1016/j.mattod.2020.06.003

the rising or falling velocity of liquid level is usually lower than 6 mm/s, and therefore the floater speed can be accurately measured with a minor measurement error, meeting the practical requirements.

Liquid level real-time monitoring and automatic control system

Liquid substances are extensively applied in various fields from individual daily life to mass production, where the liquid level and flow rate are two important flow parameters needing to be

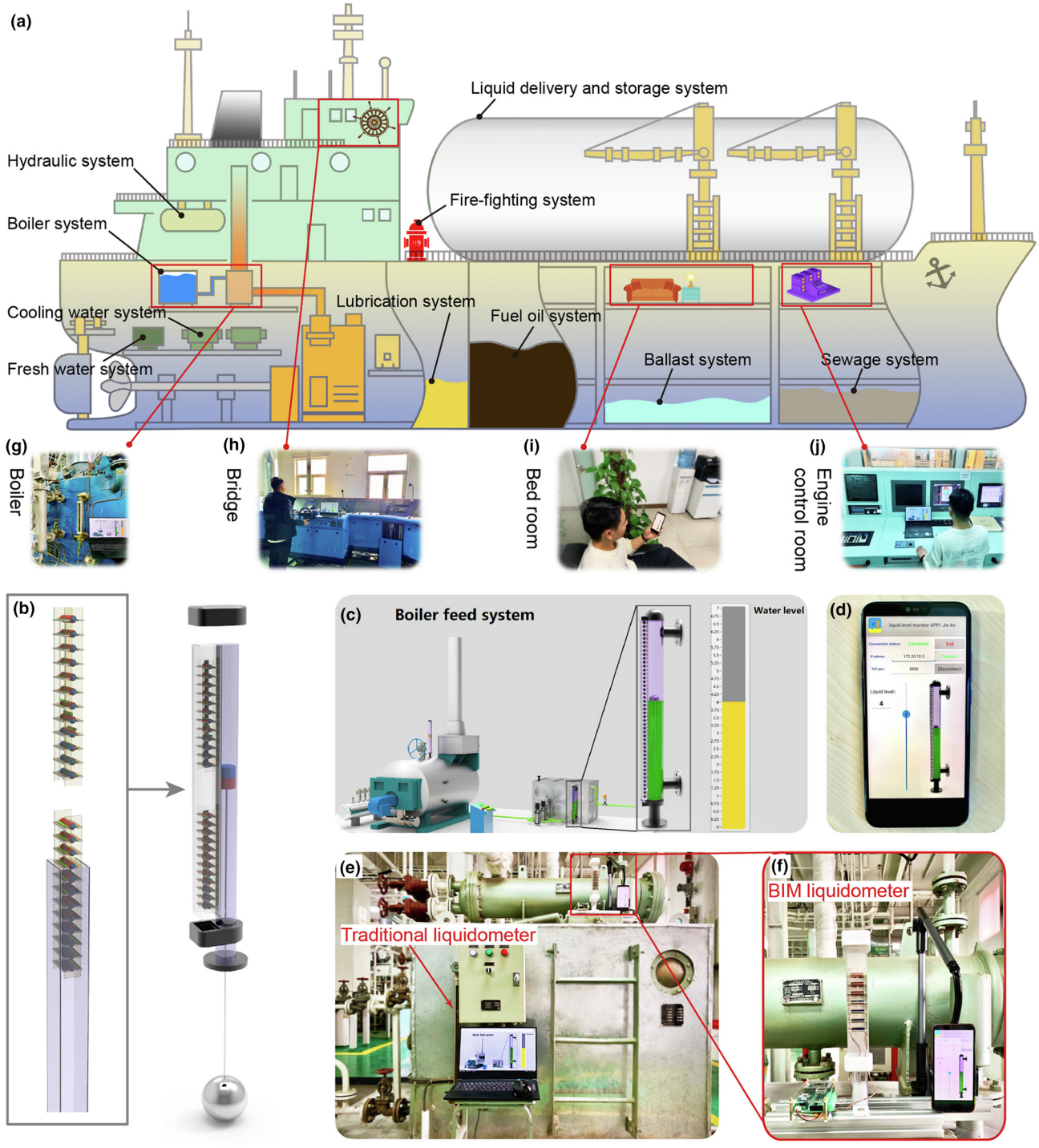

FIGURE 6

Practical application of water level monitoring for a boiler feed tank in a ship engine room. (a) Schematic diagram of ship systems requiring liquid level or flow rate monitoring. (b) Assembly diagram of top-mounted liquidometer used in this practical application due to its simple installation and heat insulation. (c) Computer monitoring program interface of boiler feed water system. (d) Mobile app for portable remote monitoring of water level in a boiler feed tank. (e) Panoramic photo of the experiment device site and (f) partially enlarged view near the liquidometer. Equipped with the BIM liquidometer, the water level information of the boiler feed tank can be monitored in real time: (g) near the boiler, (h) in bridge, (j) in engine control room, and even (i) in one's bedroom.

Please cite this article in press as: J. An et al., Materials Today (2020), https://doi.org/10.1016/j.mattod.2020.06.003

reliably detected. Unlike the sensors for personal devices, industrial sensors are often required to have easy troubleshooting, long operation life, adaptability, and improved reliability under harsh working conditions such as elevated temperature, high atmospheric pressure, corrosion, and wearing [29]. These requirements make a majority of systems with electronic sensors have to cooperate with auxiliary mechanical sensors. The BIM panel can serve as both a reliable mechanical indicator and an electrical sensor under vibration, humid environment, and high temperature liquid, as shown in Fig. S8. It can indicate the liquid level and flow rate information based on the color difference of flaps and also act as an electrical sensor for remote monitoring and electric control. With the advantages of mechatronic sensors, the BIM liquidometers are a promising candidate for level monitoring and automatic control in water, fuel, and lubricant oil tanks. Fig. 4a shows the schematic diagram of a proposed boiler feed water system which is universally used in power stations and chemical plants. The system consists of two main parts: boiler and filling tank, both of which requires liquidometers to monitor the water level. A BIM liquidometer is mounted on the top of the boiler to prevent the liquidometer from overheating by decreasing the heat transfer, and the other is mounted on the side of water feeding tank to save space. These two installation methods are selected according to the practical requirements. The preheated water in the water feeding tank is pumped into the boiler to generate steam, providing temperature and power for industrial manufacture. When the water level of filling tank falls to the minimum value, the inlet valve will be opened to replenish water until the level rises back to the maximum value. This process, which is called liquid level two-position control runs automatically through the automatic control cabinet, and the control process in boiler is basically identical. In order to simulate a practical scenario, we constructed a similar filling tank to demonstrate the practical applications of the BIM liquidometer in liquid level two-position control, as shown in Fig. 4b. Water can be drained from the manual drain valve to simulate the water consuming by the boiler and an electric valve is used to realize the automatic replenishment of the water in the feeding tank (Fig. 4c). The integrated BIM liquidometer with six flap units was capable of realizing the two-position control of liquid level, in which the flap number can be adjusted according to the application environment. When the liquid level rises through a flap, a positive peak of dV/dt is generated, and, conversely, a negative peak can be detected during the falling process. If the liquid level stops at a middle position, a zero domain appears between two groups of positive peaks in the dV/dt signal (Fig. 4d). A LabView program was developed to acquire and process the measured voltage signal and realize the two-position control of liquid level. The program interface is exhibited in the inset of Fig. 4a and Fig. S9a, which can display the acquired electrical signals and processed numerical results, including real-time moving velocity, direction of liquid level, inlet valve status, and the liquid level value. This program differentiates the acquired voltage signal, outputs filtered dV/dt signal, and then uses a peak acquisition algorithm to respectively identify the numbers of positive and negative peaks of dV/dt signal. After obtaining liquid level value by analyzing peak numbers in real time, the program can further take appropriate control according to the current liquid level. If the liquid level is below the low setting level, the system will send a red alarm signal and open the electric inlet valve automatically to replenish water until the level arrives at the high setting level. Such a simple control algorithm can stabilize the level between two setting values and realize the liquid level two-position control (Fig. 4e). This process is shown in Fig. 4f–n and Movie S2. The BIM liquidometer exhibits high reliability from the good matching between the local displays and the remote monitoring system.

Flow rate remote monitoring and control system

Flow rate is another important parameter which needs to be monitored in broad practical situations. Therefore, a BIM flowmeter assembled by a magnetic flap panel, floater, and conical chamber was designed as shown in Fig. 5a. We also designed a signal processing and wireless transmission module (SPWTM) integrated with 10-channel signal acquisition circuit to continuously scan the voltage signal from each flap unit (Fig. 5b and Fig. S9c). Fig. 5e illustrates the voltage signals of four channels during one rising-falling cycle. Through the order in which the channel signal exceeds the preset threshold, the floater location can be determined. According to one-to-one correspondence between the floater location and flow rate in conical chamber, real-time flow rate information can be acquired. The flow rate information can be wirelessly transferred to terminal equipment, such as smart phones, laptops, or an external server, through a router (Fig. 5c) and form a liquid flow remote monitoring and control system (Fig. 5a and Fig. S9b). Meanwhile, the terminal equipment can also send a command to control the liquid flow remotely. When the SPWTM receives this command containing the flow setting value via the WIFI connection, it will employ a proportion integration differentiation (PID) algorithm and negative feedback method to control the valve opening and stabilize the water flow at the set value. In this PID control process, the SPWTM also wirelessly sends real-time water flow information to a computer program for real-time remote monitoring (Fig. 5d and Movie S3). The BIM liquidometer and flowmeter, as two reliable electromechanical liquid sensors, will have promising prospects in many applications such as transportation, oil exploitation, sewage treatment, chemical industry, and even household appliances (Fig. 5f). This work lays the foundation for TENG-based active sensors in liquid monitoring and control and will further promote the development of smart cities, factories, and transportation.

Practical application of water level monitoring in a boiler feed tank in ship engine room

A whole ship system resembles a mobile city with considerable complexity and is usually classified into five major systems according to the working medium, as schematically shown in Fig. 6a. There are a large number of systems on ships which require real-time monitoring through sensors to ensure system safety (Fig. S10). Taking the boiler feed water system as an example, as the water shortage in the boiler will cause it to be burnt out, it is necessary to monitor the system in real time to ensure that there is a sufficient amount of water in the boiler feed tank. In order to demonstrate the practicality of a developed sensor in

Please cite this article in press as: J. An et al., Materials Today (2020), https://doi.org/10.1016/j.mattod.2020.06.003

such demanding environments as ships, a top-mounted BIM liquidometer with the advantages of simple installation and heat insulation was utilized in this system for monitoring the liquid level variation. The simple and efficient assembly process of the liquidometer is beneficial as it can be easily maintained and repaired by crews during the voyage, and the flap units can be easily spliced benefiting length customization (Fig. 6b). The well-designed computer program can be used as the control and monitoring center to acquire the sensing signals and regulate the entire boiler feed system (Fig. 6c). Besides, a mobile application was also developed for portable remote monitoring of various parameters in the system (Fig. 6d and Fig. S9d). The panoramic photo of the experiment device site is shown in Fig. 6e. The liquid level information can be read directly from the liquidometer panel and acquired remotely from mobile terminals such as mobile phones or personal computers (Fig. 6e, and Movie S4). All monitoring terminals and sensors have been connected into a unified system by the local area network on the ship. Therefore, the water level information of a boiler feed tank can be monitored in real time near the boiler and in the bridge, engine control room, and even one's bedroom (Fig. 6g–j). Further, with the continuous development of technology, an increasing number of systems will be connected into this network, and eventually, ships can be piloted automatically and remotely through satellite communication.

Conclusions

In summary, we have constructed a facile-to-fabricate TENG-based block-inserting mechatronic indicator panel for self-powered liquid level and flow rate monitoring. Owing to its unique structural design, it not only inherits the stability and reliability from mechanical sensors but also attains the ability of electrical signal transmission for electric control and remote monitoring. The simple and efficient block-inserting assembly methodology is beneficial as it can be easily maintained and repaired by crews, especially in case of an accident, and can also significantly reduce the production cost and facilitate the length customization. More importantly, the maximum measurement error does not exceed the distance between two flaps (0.8% for the panel with a flap distance of 16 mm, in a 2 m-high measured tank), which can be reduced easily by increasing the density of flaps. Panels with reasonable flap density can be conveniently customized according to the actual measurement accuracy requirement. Equipped with the BIM panel, a liquid level control system and liquid flow monitoring system were established for automatic control and wireless monitoring of water level and flow rate in real time, demonstrating its practicability in transportation, oil exploitation, sewage treatment, chemical manufactory, and other industry applications. We expect that, with an increasing number of mechatronic sensors being invented and connected into a centralized control network, the automatic driving and remote control for ships and factories could eventually be accomplished in future.

Declaration of Competing Interest

The authors declare that they have no known competing financial interests or personal relationships that could have appeared to influence the work reported in this paper.

Acknowledgements

Our thanks for the Support from the National Key R & D Project from Minister of Science and Technology (2016YFA0202704), National Natural Science Foundation of China (Grant No. 51432005, 51702018, 51561145021, and 51879022), China Postdoctoral Science Foundation (Grant No. 2019M660766), and Youth Innovation Promotion Association, CAS.

Appendix A. Supplementary data

Supplementary data to this article can be found online at https://doi.org/10.1016/j.mattod.2020.06.003.

References

[1] A.L. Fogel, J.C. Kvedar, NPJ Digit. Med. 1 (2018) 5.
[2] E.H.P. Jaramillo, Science 364 (6438) (2019) 326.
[3] D. Elger et al., Energy 2 (3) (2013) 01.
[4] V.C.G.G.P. Hancke, IEEE Trans. Ind. Electron. 56 (10) (2009) 4258.
[5] NaiqianZhang, MaohuaWang, N., Comput. Electron. Agric. (2006) 50 (1), 1..
[6] R.Y. Zhong et al., Engineering 3 (5) (2017) 616.
[7] Z.L. Wang, Mater. Today 20 (2) (2017) 74.
[8] Z.L. Wang, Nano Energy (2019) 104272.
[9] H. Guo et al., Sci. Robot. 3 (20) (2018) eaat2516.
[10] J. Luo et al., Nat. Commun. 10 (2019) 1.
[11] Y. Zou et al., Nat. Commun. 10 (1) (2019) 2695.
[12] J. Nie et al., Nat. Commun. 10 (1) (2019) 2264.
[13] P. Jiang et al., Adv. Mater. (2019) e1902793.
[14] K. Dong et al., Adv. Mater. (2019) e1902549.
[15] X. Pu et al., Sci. Adv. 3 (7) (2017) e1700694.
[16] F. Xi et al., Nano Energy 61 (2019) 1.
[17] L. Cheng et al., Nat. Commun. 9 (1) (2018) 3773.
[18] C. Zhang et al., Adv. Mater. 26 (22) (2014) 3580.
[19] W. Li et al., Nat. Commun. 8 (2017) 15310.
[20] Z.L. Wang, Nature 524 (2017) 295.
[21] X. Xiao et al., Adv. Energy Mater. (2019) 1902460.
[22] Z.L. Wang et al., Energy Environ. Sci. 8 (8) (2015) 2250.
[23] W. Liu et al., Nat. Commun. 10 (1) (2019) 1426.
[24] H. Zou et al., Nat. Commun. 10 (2019) 1.
[25] F.-R. Fan et al., Nano Energy 1 (2) (2012) 328.
[26] C. Xu et al., Adv. Mater. 30 (15) (2018) e1706790.
[27] S. Lin et al., Adv. Mater. 31 (17) (2019) e1808197.
[28] S. Lin et al., Adv. Mater. (2019) e1901418.
[29] J.F. Vesecky et al., IEEE 3 (2009) III.

Please cite this article in press as: J. An et al., Materials Today (2020), https://doi.org/10.1016/j.mattod.2020.06.003